# Ab initio study of chemical species in the BCl 3 plasma: Structure, spectra, and decomposition paths

Kyoung K. Baeck and Rodney J. Bartlett

Citation: The Journal of Chemical Physics **106**, 4604 (1997); doi: 10.1063/1.473986
View online: http://dx.doi.org/10.1063/1.473986
View Table of Contents: http://scitation.aip.org/content/aip/journal/jcp/106/11?ver=pdfcov
Published by the AIP Publishing

# *Ab initio* study of chemical species in the $BCl_3$ plasma: Structure, spectra, and decomposition paths

Kyoung K. Baeck[a] and Rodney J. Bartlett
*Quantum Theory Project, University of Florida, Gainesville, Florida 32611*

(Received 22 June 1995; accepted 11 December 1996)

Industrially important plasmas offer a variety of complicated molecular processes that benefit from predictive quantum chemical techniques. *Ab initio* coupled-cluster and MBPT methods are used to characterize structures, vibrational frequencies, ionization potentials, electron affinities, and excited states for the main fragments in the $BCl_3$ plasma, i.e. $BCl_3$, $BCl_2$, BCl, and their anions and cations for which few experimental results exist. The excited, electron attached, and ionized states are calculated by employing the equation-of-motion coupled cluster (EOM-CC) method. Recent results from a photofragmentation study and an electron collision experiment are analysed based on the calculated results. Some features of the potential energy surfaces of excited states of $BCl_2$ are discussed in order to explain the origin of the experimental fluorescence spectrum. We also consider possible microscopic processes with low energy, such as the formation and destruction of neutral and ionic species, decomposition paths, and the role of each fragment. While decomposition through transient states of $BCl_3^-$ by electron attachment is the most probable path for low-energy electron attachment, decomposition through excited states of $BCl_3$ can play a role only when there is no other way to make the $BCl_3^+$ ion. © *1997 American Institute of Physics.* [S0021-9606(97)01711-X]

## I. INTRODUCTION

The boron trichloride ($BCl_3$) molecule is of considerable recent interest because of its use in radio-frequency (rf) plasmas, which are widely used in the commercial etching of metals and semiconductors such as Al, $Al_2O_3$, Si, and III–V compound materials.[1–4] Yet little is known about $BCl_3$ and its fragments. Several models for plasma processes have been proposed,[5–7] and some of them attempt to explain the complex chain of processes in a $BCl_3$ discharge.[8,9] Such modeling, however, is based on very limited experimental data, since an inadequate explanation is available about the detailed microscopic mechanisms.

In the underlying plasma chemistry,[5] radicals and charged fragments are created and destroyed by a wide variety of atomic and molecular processes. Much information is required about the way and the rate at which these reactions occur. Such data, sometimes extrapolated from results for simpler experimental conditions,[10] are used in several kinds of macroscopic plasma models. These include the particle in a cell Monte Carlo collision model (PIC/MCC)[11] and the Boltzmann equation and fluid method.[12] Such models attempt to describe the relation among the experimental conditions for dry etching, but are hindered by the lack of fundamental data. Although new techniques,[13–15] such as the application of laser spectroscopy to gas discharges by laser induced fluorescence, have become major methods to obtain information about the basic processes, the identity and role of the various fragments still remain vague. As the chemical species in a plasma mixture are unstable, very reactive, and difficult to handle separately, experimental studies are difficult, and only limited experimental results are available.

In order to understand (and model) the basic chemistry in a plasma process, several experimental results obtained by different methods must be integrated. But the lack of substantial information, which is rather difficult to obtain by experimental methods, recommends the application of predictive theoretical methods. Theory requires both electronic structure results for potential energy surfaces and the application of scattering theory to obtain cross sections. In this paper, we focus on the first aspect.

In order to uncover the basic processes in the $BCl_3$ radio-frequency plasma, many experimental kinetics studies[16] and spectroscopic investigations[17] have recently been conducted. The Penning ionization of $BCl_3$[18] by metastable argon, $Ar_m$, followed by dissociative recombination of $BCl_3^+$ with an electron,[19]

$$BCl_3 + Ar_m \rightarrow (BCl_3)^*, \quad Ar \rightarrow BCl_3^+ + Ar + e^-, \tag{1}$$

$$BCl_3^+ + e^- \rightarrow (BCl_3)^* \rightarrow BCl(X^1\Sigma^+, A^1\Pi) + 2Cl, \tag{2}$$

is supposed to be one of the most probable processes for the electron impact dissociation of $BCl_3$. Experimental efforts to verify such complex kinetic processes are dependent on monitoring BCl by its spectroscopic signal for the $A^1\Pi \rightarrow X^1\Sigma^+$ transition.

Though $Cl^-$ is the major negative species detected experimentally, there is some experimental evidence[20,21] that shows that $BCl_3^-$ is the initial product of the low-energy electron attachment of $BCl_3$. Thus, the following dissociative electron attachment process is likely to be another major process:[22]

$$BCl_3 + e^- \rightarrow BCl_3^-, \tag{3}$$

[a]Permanent address: Department of Chemistry, Kangnung National University, Kangnung 210–702, Korea.

$$BCl_3^- \rightarrow BCl_2 + Cl^-, \quad (4)$$

$$BCl_3^- \rightarrow BCl(X^1\Sigma^+, A^1\Pi) + 2Cl + e^-. \quad (5)$$

It is now well accepted that many of the free electrons in radio-frequency plasmas are secondary electrons, i.e., low-energy electrons which can initiate the above process. There are also some spectroscopic studies for the $BCl_2$ fragments obtained from $BCl_3$.[23,24]

Despite the above facts and many experimental efforts, questions and discrepancies remain between experimental results for the identity and role of negative ions and fragments in the $BCl_3$ plasma processes, in particular, the role of $BCl_3^-$ is not well established. Consequently some recent experimental results on the $BCl_3$ discharge systems are not fully understood and not used to model the plasma process because of an inadequate understanding of the experimental results.

To understand the initial steps of the above processes and the experimental results, we require substantial basic information about $BCl_3$ and its fragments, not only for the ground state, but for the excited states. While the spectroscopy for the excited states is governed by selection rules in optical excitation, optically forbidden states can play a role in plasma processes. For a complete description of the role of excited states in a plasma process, additional information about non-optically allowed states is pertinent. Considering the importance of these basic data, it is suprising that there are only a few reliable experimental results[24–26] for the geometric and spectroscopic properties of $BCl_3^-$, $BCl_3^+$, $BCl_2^-$, $BCl_2$, $BCl_2^+$, $BCl^-$, and $BCl^+$.

Previous theoretical studies for $BCl_3$ have been limited to semiempirical calculations,[27] some SCF calculations,[28] and the multiple scattering $X\alpha$ method,[29] all limited to the ground state of $BCl_3$. No theoretical calculations for $BCl_3^-$ and other fragments have been reported to date.

We characterize all neutral and ionic species in the $BCl_3$ plasma, i.e., the structure, excited electronic states, spectroscopic properties, and possible decomposition processes, with MBPT(2) and coupled-cluster methods, CCSD and CCSD(T),[30] with the ACES–II program system.[31] The equation-of-motion (EOM-CC) methods[32] are used to calculate ionization energies,[33] electronic excitation energies,[32] and electron attached processes.[34] Force constants are calculated by finite differentiation of the analytically computed derivatives.[35] Based upon the calculated results, we consider some possible microscopic processes, such as the formation and destruction of ionic species, the decomposition path, and the role of each fragment.

The actual diversity of chemical reactions and the dominant chemical processes in a plasma mixture depend largely on the average energy of the electrons in the plasma. The higher the average energy of the electrons, the more complicated the chain of reactions involved. In order to understand the initial steps in the $BCl_3$ plasma, we consider all species that occur in chemical processes with reaction energies less than 11 eV. Though this energy range is small compared to the average energy of electrons in the usual radio-frequency plasma etching where the main excitation sources are low-energy electrons up to 30 eV, even the reactions and species in this energy range are not understood experimentally. A greater knowledge of these low energy collisions may help to design more effective plasma processes that reduce harmful effects on substrates.

TABLE I. Electron affinities (eV) of Cl and $Cl_2$ by the CCSD method.

| Core | Valence | | EA(Cl) | AEA($Cl_2$)[e] |
|---|---|---|---|---|
| ECP-1[a] | VAL-1[a] | Basis-I | 3.163 | 2.460 |
| ECP-2[b] | VAL-2[b] | | 2.147 | 2.378 |
| ECP-2 | VAL-1 | Basis-II | 3.333 | 2.541 |
| ECP-3[c] | VAL-3[c] | | 2.403 | 1.948 |
| ECP-3 | VAL-1 | | 3.333 | 2.528 |
| Experimental values | | | 3.613[d] | 2.380[e] |

[a]ECP by Dolg (Ref. 38) with a (6,6,1)/[3,3,1] valence basis set.
[b]ECP by Wadt and Hay (Ref. 39) with (3,3)/[2,2] valence basis set.
[c]ECP by Pacios and Christiansen (Ref. 40) with a (4,4,1)/[4,4,1] valence basis set.
[d]Electron affinity of Cl (Ref. 41).
[e]Adiabatic electron affinity (Ref. 42).

## II. BASIS SET SELECTION AND COMPUTATIONAL METHODS

In order to properly describe the electronic states of negative ions, the basis set selection is very important, especially when the electronic affinity is small.[36] The small experimental electron affinity of $BCl_3$[37] requires a careful choice of basis set. An all-electron basis for $BCl_3$ is, however, rather large for geometry optimization, calculation of excited states, and the study of decomposition potential surfaces. This recommends the use of an effective core-potential (ECP) and associated basis set. Although the relativistic effect is not expected to be large in this system, some relativistic effects can also be included by using the effective core-potential.

In order to select the proper basis set, the basis set dependence of the electron affinity of Cl and $Cl_2$ are calculated with some combinations of ECP's and valence basis sets. The adiabatic electronic affinity of $Cl_2$ is obtained as the difference in total energy between $Cl_2$ and $Cl_2^-$ with the CCSD method at their respective MBPT(2) geometries. The results are given in Table I and compared with the experimental results. The ECP and valence basis set (Basis-I) by Dolg[38] produce the lowest total energies for Cl, $Cl^-$, $Cl_2$, and $Cl_2^-$. So this will serve as the first choice for the study of $BCl_3$ and its fragments. Because of the small value of the experimental electron affinity of $BCl_3$, $0.33 \pm 0.2$ eV,[37] another combination of ECP and valence basis set (Basis-II) that produces the largest value for the electron affinity of Cl and $Cl_2$ is taken as a second choice. The basis set dependence of calculated results like geometries, vibrational frequencies, and excitation energies, will be obtained with the two different basis sets. It should be noted that the 3.6 eV electron affinity of Cl is underestimated by these ECP basis sets by 0.45 eV with Basis-I and 0.28 eV with Basis-II.

To ensure a balanced description of the electron cloud in the bonding region and the correlation calculations, a PVDZ

TABLE II. BCl. The three entries for the bond length ($R_e$) correspond to the results by MBPT(2), CCSD, and CCSD(T) methods, respectively. The vibration frequencies ($\nu$) are calculated by the MBPT(2), CCSD, and CCSD(T) methods all at their respective geometries. The vertical transition energies ($T_e'$) for BCl are calculated at the MBPT(2) geometry.

| Basis | | $\nu$ | $T_e'$ (eV)[b] | |
|---|---|---|---|---|
| sets | $R_e$ (Å) | $cm^{-1}$ | $^3\Pi \leftarrow {}^1\Sigma^+$ | $^1\Pi \leftarrow {}^1\Sigma^+$ |
| Basis-I | 1.742,1.753,1.755 | 842,826,821 | 2.54(2.56)[c] | 4.89(4.90)[c,d] |
| Basis-II | 1.747,1.757,1.759 | 847,833,829 | 2.51(2.53)[c] | 4.89(4.90)[c,d] |
| PVDZ | 1.730,1.741,1.743 | 869,851,846 | 2.54(2.56)[c] | 4.87(4.88)[c,d] |
| 6-31G* | 1.714,1.724,1.726 | 880,865,860 | 2.42(2.43)[c] | 4.96(4.98)[c,d] |
| PVTZ | 1.708,1.718,1.720 | 869,854,849 | 2.49(2.52)[c] | 4.67(4.70)[c,d] |
| Expt[a] | 1.716 | 843 | 2.50 | 4.55 |

[a]Experimental value from Herzberg (Ref. 51).
[b]Calculated by the EOM–CCSD method (Ref. 32).
[c]Calculated as the difference between the CCSD(T) (Ref. 45) energies.
[d]The multireference, TD-CCSD method (Refs. 49 and 50) is used for the $^1\Pi$ state.

basis set $[3s2p1d]$ by Dunning[43] is selected for the B atom, to be consistent with the valence basis for the Cl atom by Dolg,[38] VAL-1, which consists of a $[3s3p1d]$ basis. The basis sets PVDZ for the B atom and ECP-1/VAL-1 (Basis-I) and ECP-2/VAL-1 basis set (Basis-II) for the Cl atom are used throughout this work. The PVTZ all-electron basis sets,[43] $(10s,5p,2d,1f)/[4s,3p,2d,1f]$ for B and $(15s,9p,2d,1f)/[5s,4p,2d,1f]$ for Cl, are also used for smaller molecules like BCl and $BCl_2$.

All of the following MBPT(2) and coupled-cluster single and double (CCSD)[44] calculations including noniterative triple excitations [CCSD(T)][45] use a RHF reference function for closed-shell molecules and UHF reference functions for the open-shell systems. When the UHF reference function is used, the possibility of spin-contamination is checked, and there was no case of noticeable spin contamination. For example, in the case of $BCl_3^-$, the projected spin multiplicity[46] in MBPT(2) and CCSD results was $2.000 \pm 0.001$ in all cases. As demonstrated in the previous work,[47] the effects of spin contamination on results should not be significant at the coupled-cluster level.

Excitation energies are calculated by the equation-of-motion coupled-cluster single and double (EOM-CCSD) method.[32,34] The value of the approximate-excitation-level (AEL)[32] falls between 1.04 and 1.12 in all calculations reported here. Excited states are fairly well described by the EOM-CCSD method when the AEL value is close to 1.0.

## III. $BCl^+$, BCl, AND $BCl^-$

As a simple test for the choice of the above basis set, we report in Table II bond lengths, vibrational frequencies, and vertical excitation energies [the latter at MBPT(2) geometries] with all-electron basis sets and the two ECP-associated basis sets.

While the difference between the bond length with MBPT(2), CCSD, and CCSD(T) is about 0.01 Å, the difference caused by the different basis sets is about 0.03 Å. Compared with the experimental bond length of BCl, 1.716 Å, the calculated value with Basis-I is longer by about 0.03 Å. This might be partially due to the neglected core–valence correlation effect and partially because of inadequate basis sets for the valence part. Based on these data, the optimized geometries with the MBPT(2) method with the ECP and associated valence basis set can be expected to be accurate to about 0.03 Å in the BCl systems.

The vertical excitation energies in Table II are calculated by the EOM-CCSD method[32] and by the difference between total energies by the CCSD(T) method[45] for each state. The two-determinant TD-CCSD method[49] argumented with triples[50] is used for the singlet open-shell state, $^1\Pi$. The effect of triple excitations estimated by CCSD(T) is less than 0.03 eV. Though the numbers are not given in the table, the excitation energies calculated by the same methods at the CCSD(T) geometry differ from the values in the table by less than 0.01 eV. While the calculated value for the $^3\Pi \leftarrow {}^1\Sigma^+$ excitation shows good agreement with the experimental value, those for $^1\Pi \leftarrow {}^1\Sigma^+$ show a little larger deviation. The better agreement with the results with the PVTZ basis set[43] means that the main source of error is the basis rather than the correlated method. The larger computed excitation value for the $^1\Pi \leftarrow {}^1\Sigma^+$ transition means that the excited state $^1\Pi$ is probably not as well described as is the ground state in the basis, which might be related to the basis set deficiency on the B atom as in the case of the electron affinity.[36] This deficiency is expected to be abbreviated in the $BCl_3$ system because of the Cl basis functions. While the 6-31G* basis set[48] results are better for bond lengths, the PVDZ basis set[43] gives slightly better results for the excitation energies. The ECP-associated basis set, Basis-I, reproduces quite well the bond length and the excitation energies calculated by the all electron PVDZ basis set.

The vertical electronic transition energies of BCl calculated by the EOM-CCSD method[32] with Basis-I (Basis-II) at the optimized bond length with MBPT(2) are 2.54 (2.51) eV and 4.89 (4.89) eV for $A^1\Pi \leftarrow X^1\Sigma^+$ and $a^3\Pi \leftarrow X^1\Sigma^+$ transitions, respectively. The approximate- excitation-levels[32] in the EOM-CCSD calculations are between 1.03 and 1.09. The experimental transition energies are 2.50 eV and 4.55 eV, respectively.[51] In order to make a direct comparision between the experimental value and the calculated result, we have to consider not only the limitations of the present calculation method, such as the core–valence correlation effect, the finite basis-set size, and the level of correlation, but also some other factors such as the effect of the vibrational energy level and the change in geometry between the ground state and the excited states. The experimental bond lengths and vibrational frequencies of each state, $X^1\Sigma^+$(1.716 Å, 839 $cm^{-1}$), $a^3\Pi$(1.698 Å, 911 $cm^{-1}$), $A^1\Pi$(1.689 Å, 849 $cm^{-1}$), are very similar. Therefore, the error of the present method for the excitation energy, i.e., the EOM-CCSD// MBPT(2) calculation with the PVDZ basis set for the B atom and the ECP-1/VAL-1 basis set for the Cl atom, can be estimated to fall within a few tenths of an eV.

The next excited states are also calculated by the EOM-CCSD method. The third and the fourth excited states are triplet states and the main electronic transition is $\pi \rightarrow \pi^*$.

TABLE III. $BCl^+$. Bond lengths and vibration frequencies calculated with Basis-I, Basis-II, and the PVTZ all-electron basis set. The three entries in each item represent the results by MBPT(2), CCSD, and CCSD(T) methods, respectively.

| | $BCl^+(^2\Sigma)$ | | IP(eV)[a] | |
|---|---|---|---|---|
| | $R_e$ (Å) | $\nu$ ($cm^{-1}$) | Vertical | Adiabatic |
| Basis-I | 1.618,1.622,1.626 | 1156,1126,1115 | 10.09 | 9.87 |
| Basis-II | 1.620,1.623,1.628 | 1171,1146,1131 | 10.17 | 9.93 |
| PVTZ | 1.595,1.597,1.602 | 1179,1158,1143 | 10.17 | 9.93 |
| (Exp) | | | (10.26)[b] | (9.03)[c] |

[a]Vertical and adiabatic ionization potential and electron affinity for BCl. IP and EA are calculated as the difference between the CCSD(T) energies at the MBPT(2) geometry.
[b]Thermodynamically estimated value (Ref. 24).
[c]From the absorption spectrum of the BCl molecules (Ref. 53).

These two states are the $^3\Sigma^+$ or $^3\Delta$ states. The excitation energies for the two states are 6.98 eV and 7.35 eV, respectively.

While the ground state of BCl is $^1\Sigma^+$ with a $\sim 6\sigma^2 2\pi^4 7\sigma^2$ electronic configuration, the ground state of $BCl^+$ is $^2\Sigma$ with a $\sim 6\sigma^2 2\pi^4 7\sigma^1$ electronic configuration. The bond length and vibrational frequencies, the ionization potential (IP), and the electron affinity (EA) are calculated with the two ECP basis sets and the PVTZ basis sets, and the results are given in Table III. The bond length and frequency of $BCl^+$ in the JANAF table[52] is estimated to fall between the value for BCl and BeCl. The estimated values, 1.73 Å and 845 $cm^{-1}$, are far from the calculated results. Compared to BCl, the shorter bond length and the higher vibrational frequency of $BCl^+$ imply that the HOMO (highest occupied molecular orbital) of BCl has some antibonding character.

The ionization potential and electron affinity of BCl are obtained by the difference between the total energy with the CCSD(T) method at the MBPT(2) geometry. Considering the accuracy in the calculated ionization potentials, which will be established further in the next section, the experimentally estimated ionization potential of BCl, 11.3 eV in the JANAF table, is rather large compared to the calculated ionization potentials, 10.2 eV for the vertical and 9.9 eV for the adiabatic ionization. A recent experimental result[53] estimated the IP of BCl to be 9.03 eV, which we doubt.

There is no experimental evidence for the existence of the $BCl^-$ ion in the $BCl_3$ plasma. According to the present calculation, this negative ion is unstable relative to the neutral molecule, but the absolute value of the calculated electron affinity is very small, and the temporary existence of metastable $BCl^-$ might be expected.

## IV. $BCl_2^+$, $BCl_2$, AND $BCl_2^-$

From the mass spectrometric study of photoionization,[55] $BCl_2^+$ was detected from $BCl_3$ at a threshold energy of 12.30 eV. A recent fluorescence study[23,24] showed that some excited states of $BCl_2$ derive from $BCl_3$. Though there are no explicit experimental results, $BCl_2^-$ can be expected to be involved in the $BCl_3$ plasma. However, the exact characteristics and properties of these molecules are only addressed by a few experiments[25] because of their transient nature.

The bond lengths, angles, and vibrational frequencies in Table IV are calculated at the MBPT(2) level with Basis-I and using the PVTZ[43] all-electron basis set.

$BCl_2$ has a $C_{2v}$ structure, and the ground state of $BCl_2$ is the $X^2A_1$ state having a single electron in an $a_1$ orbital. To see the effect of basis set size, the geometry and vibrational frequencies are computed with PVTZ[43] all-electron basis sets at MBPT(2). Optimizing the geometry with a 6-31G* basis and the CCSD(T) method offers an estimate of the effect of correlation on the geometry. The ten core molecular orbitals are frozen in the analytical gradient correlated calculation[57]

TABLE IV. MBPT(2) bond lengths ($R_e$ in Å), bond angles ($\angle$ in degrees), and vibration frequencies ($\nu$ in $cm^{-1}$) for $BCl_2^+$, $BCl_2$, and $BCl_2^-$ ($X^1A_1$ and $a^3B_2$ states). The two entries in each item are, respectively, the results from Basis-I and the PVTZ basis set.

| | | $BCl_2^+$ $X^1\Sigma_g^+$ | | $BCl_2$ $X^2A_1$ | $BCl_2^-$ $X^1A_1$ | $BCl_2^-$ $a^3B_2$ |
|---|---|---|---|---|---|---|
| $R_e$ | | 1.633,1.610 | | 1.746,1.720 (1.728)[a] | 1.962,1.894 | 1.881,1.838 |
| $\angle_{ClBCl}$ | | 180,180 | | 124.6,125.1 (125.6)[a],(121)[b] | 101.7,103.2 | 117.4,118.6 |
| | $\nu(\sigma_g^+)$ | 564,577 | $\nu(a_1)$ | 286,290 | 242,259 | 223,235 |
| | $\nu(\sigma_u^-)$ | 1458,1489 (1436.3)[d] | $\nu(a_1)$ | 722,722 (731)[b] | 556,567 | 591,603 |
| | $\nu(\pi_u)$ | 312,372 | $\nu(b_1)$ | 997,1012 (967)[b] | 453,525 | 706,748 |
| IP/EA(eV)[c] | | | | | | |
| Vertical | | 8.61,8.66 | | | 0.23,0.26 | −0.18,−0.37 |
| Adiabatic | | 7.16,7.16 | | | 1.35,1.09 | −0.05,−0.06 |

[a]Result of a CCSD(T) calculation with the 6-31G* basis set. Ten core molecular orbitals are frozen in the analytic gradient calculations with the CCSD(T) correlation method (Ref. 57).
[b]Experimental values from radiolysis and photolysis (Ref. 25).
[c]Vertical and adiabatic ionization potentials and electron affinities for $BCl_2$, calculated as the difference between the CCSD(T) energies at the MBPT(2) geometry.
[d]Experimental results from Ref. 26.

in the 6-31G* basis. The calculated bond lengths in Table IV are very similar to the estimated value in the JANAF table 1.73 Å, while the bond angle is a little larger than the JANAF estimate 112°, but close to the predicted value from the recent experiment,[25] 121°. Simply speaking, the geometry of $BCl_2$ is almost the same as that of the $BCl_2$ moiety of $BCl_3$. The calculated vibrational frequencies for the second and third mode are very close to the experimental values,[25] 731 and 967 $cm^{-1}$. For the first IR band, which is not yet observed, the calculated value should be helpful in detecting the signal experimentally.

$BCl_2^+$ has a linear structure and the ground state is $X^1\Pi_g^+$ with a $\sim 11\sigma^2 3\pi^4 4\pi^4$ electronic configuration. The estimated bond length (1.74) and vibrational frequencies (500, 800, and 150 $cm^{-1}$) in the JANAF table are rather far from the calculated results in this case, except the first vibrational frequency. According to the calculated result, the vibrational band of $\sigma_u^-$ is expected to be observed in the usual IR spectrum, and the triplet bands, 1415.3, 1417.9, and 1420.4 in the experimental results[25] are suspected to be the $\sigma_u^-$ band of $BCl_2^+$. The work of Jacox *et al.*,[26] reported after submission of this paper finds the $\nu_3$ absorption at 1436.3 $cm^{-1}$. The calculated adiabatic and vertical IP's, 7.2 eV and 8.6 eV, can be compared with the estimated value 7.71 and 7.74 eV in Ref. 24 and the JANAF table, respectively, which are obtained through a combination of experimental results by photoionization and electron impact studies. From the calculated vertical ionization potential, it is expected that $BCl_2^+$ can be formed from $BCl_2$ when the colliding electrons have an energy of more than 8.61 eV.

An additional electron in $BCl_2^-$ can either occupy the HOMO of $BCl_2$ and make a $^1A_1$ state with the $a_1^2$ configuration, or occupy the LUMO (the lowest unoccupied orbital) and make a $^3B_2$ state with the $a_1^1 b_2^1$ configuration. According to the calculated results, the $^1A_1$ state is the ground state. The first excited triplet state is $^3B_2$, as also occurs for $CCl_2$ and $SiCl_2$. The vertical singlet–triplet splitting is 0.41 eV and the adiabatic singlet–triplet splitting is 0.25 eV at the $BCl_2$ geometry. The vertical singlet–triplet splitting at the MBPT(2) geometry of the singlet state is 1.11 eV, which can be compared with the estimated value, 1.49 eV in the JANAF table. While the singlet $BCl_2^-$ is stable relative to its neutral species, the triplet $BCl_2^-$ is unstable, both vertically and adiabatically even with the PVTZ basis sets. Because the effect of the basis set is expected to be significant in these anionic systems, an extensive basis set calculation could find the $a^3B_2$ to have a small positive electron affinity. Vertical and adiabatic EA's $\sim$0.3 eV and $\sim$1.2 eV, for the $X^1A_1$ state from the present calculations, can be compared with the value 0.63 eV$\pm$1.0 eV in the JANAF table which is estimated from the comparison of the IP and EA's for isoelectronic molecules. The dissociation energy of $BCl_2^-$ into BCl and $Cl^-$ is calculated to be 0.52 eV in the PVTZ basis set.

The change in the bond length shows that the HOMO of $BCl_2$ has antibonding character while the LUMO has bonding character. Considering the differences between the results by Basis-I and the PVTZ basis sets, the results for $BCl_2^+$ and $BCl_2$ are expected to be correct within 0.02 Å in bond length and $\sim$20 $cm^{-1}$ in vibrational frequencies. The results for anionic states, however, are expected to be reliable within an estimated $\sim$0.05 Å and $\sim$40 $cm^{-1}$ error.

## V. $BCl_3^+$, $BCl_3$, AND $BCl_3^-$

The ground state of $BCl_3$ is $X^1A_1'$ of $D_{3h}$ symmetry. The order of the highest occupied orbitals, $\cdots e'e''a_2'$, and the lowest unoccupied orbitals, $a_2''a_1'e'\cdots$, are shown in Table VIII, which agrees with previous calculations.[28] From the orbital shape of $a_2''$ of $BCl_3$, which has $\pi^*$ character[58] and Walsh's rules,[59] the ground state of $BCl_3^-$ is expected to be $X^2A_1$ in $C_{3v}$ symmetry. Bond lengths and bond angles are optimized with MBPT(2) within $D_{3h}$ symmetry for $BCl_3$ and $C_{3v}$ symmetry for $BCl_3^-$. Any attempt to deviate from the given symmetry results in an increase in the energy.

In order to analyze the bonding and effects of basis sets, we consider the atomic partial charges as explained elsewhere.[60] While partial charges of the B atom and Cl atoms in $BCl_3$ are $+0.356$ and $-0.118$, respectively, those in $BCl_3^-$ are $+0.146$ and $-0.382$. Even at the $BCl_3$ geometry, the partial charges in $BCl_3^-$ are $+0.008$ and $-0.336$. The atomic partial charge is insensitive to the quality of basis set provided that the basis is not too small.[60] The negative charge in $BCl_3^-$ is delocalized mainly on Cl atoms rather than on the B atom, and the effect of the basis deficiency on the B atom is expected to be much smaller than in the $BCl^-$ and $BCl_2^-$ cases.

Because of the shape and the $\sigma^*$ character of the $a_2'$ (HOMO), the ground state of $BCl_3^+$ might be expected to be $X^2A_2'$ in $D_{3h}$ symmetry with a shorter bond length, which corresponds to a delocalized positive charge over the whole molecule. When the geometry is optimized under $D_{3h}$ symmetry, the bond length is reduced to 1.741 Å. The calculated

TABLE V. Bond length (Å) and Bond angle (°) of $BCl_3^+$, $BCl_3$, and $BCl_3^-$, by the MBPT(2) method.

| | Parameters | Basis-I | Basis-II |
|---|---|---|---|
| $BCl_3^+$ | | | |
| $C_{2v}$(2L1S)[a] | $R_{(B-Cl)}$ | 1.785,(1.789)[c] | 1.783 |
| | $R_{(B-Cl')}$ | 1.678,(1.684)[c] | 1.677 |
| | $\angle_{(ClBCl')}$ | 132.4,(132.1)[c] | 132.1 |
| | $\Delta G_0$(eV)[b] | 0.00 | 0.00 |
| $C_{2v}$(1L2S)[a] | $R_{(B-Cl)}$ | 1.696 | 1.684 |
| | $R_{(B-Cl')}$ | 1.918 | 2.078 |
| | $\angle_{(ClBCl')}$ | 111.8 | 111.4 |
| | $\Delta G_0$(eV)[b] | 0.28 | 0.55 |
| $D_{3h}$, $^2A_2'$ | $R_{(B-Cl)}$ | 1.741,(1.739)[c] | 1.740 |
| | $\Delta G_0$(eV)[b] | 0.60,(0.17)[d] | 0.59 |
| $BCl_3(D_{3h})$ | $R_{(B-Cl)}$[e] | 1.755 | 1.754 |
| $BCl_3^-(C_{3v})$ | $R_{(B-Cl)}$[f] | 1.879 | 1.876 |
| | $\angle_{(XBCl)}$[f] | 107.6 | 107.3 |

[a]The $C_2$ axis is on the B–Cl′ bond.
[b]MBPT(2) energy difference relative to the (2L1S) state.
[c]Results by the QRHF-CCSD method (Ref. 47).
[d]The QRHF-CCSD(T) (Ref. 47) energy difference relative to the (2L1S) state at the QRHF–CCSD geometry; see the text.
[e]Experimental value for $BCl_3$ (Ref. 65) is 1.751 Å.
[f]Experimental values from $Me_3P.BCl_3$ (Ref. 66) are 1.851 Å and 109.5°.

TABLE VI. Vertical ionization potential (VIP), adiabatic ionization potential (AIP), electron affinity (VEA), adiabatic electron affinity (AEA), and vertical electron detachment energy (VEDE) of the $BCl_3$–$BCl_3^-$ system obtained as the difference in the total energy at the MBPT(2) geometry. All values are in eV.

| | Basis set | SCF | MBPT(2) | CCSD | CCSD(T) | Expt. |
|---|---|---|---|---|---|---|
| VIP | I | 11.68 | 11.83 | 11.66 | 11.49 | 11.82[a] |
| | II | 11.68 | 12.34 | 11.96 | 11.79 | 11.73[b] |
| AIP | I | 11.16 | 11.44 | 11.37 | 11.29 | 11.60[a] |
| | II | 11.48 | 11.74 | 11.67 | 11.58 | 11.64[b] |
| VEA | I | −0.79 | −0.64 | −0.59 | −0.63 | |
| | II | −0.64 | −0.41 | −0.43 | −0.47 | −0.40[c] |
| AEA | I | 0.27 | 0.28 | 0.34 | 0.30 | |
| | II | 0.37 | 0.36 | 0.42 | 0.38 | 0.33 ± 0.2[d] |
| VEDE | I | 1.90 | 1.79 | 1.82 | 1.73 | |
| | II | 1.99 | 1.88 | 1.90 | 1.81 | 1.77[e] |

[a]Reference 24.
[b]Reference 71.
[c]Estimated value from the maximum cross section of negative ion formation. See the text and Ref. 21.
[d]From the charge transfer method.[37]
[e]From the optogalvanic signal.[67]

result, however, shows that the ground state of $BCl_3^+$ has $C_{2v}$ symmetry. There are two local minima in $C_{2v}$ symmetry. The first has two long and one short B–Cl bonds (2L1S), with the second the reverse. Calculated geometrical parameters are shown in Table V. According to the present results, the (2L1S) state is the ground state. The energy difference between the (2L1S) and (1L2S) configuration is calculated to be 0.28 eV with Basis-I and 0.55 eV with Basis-II. The $^2A_2'$ state in $D_{3h}$ symmetry falls 0.60 eV above the $^2B_2$ state. Some recent studies on the geometry and electronic state of the ground state of $Al_3$ showed similar problems, where the basis sets and an accurate treatment of correlation effects played an important role. While some earlier work on $Al_3$[61] supported the $C_{2v}$ structure, the most accurate experimental result[62] and theoretical study[62] confirmed that the ground state for $Al_3$ is $D_{3h}$. The same problem occurred in the $NO_3$ example,[63] where the effect of triple excitations on the correlation energy is essential to recover from the symmetry breaking.[64] As in the case of $NO_3$, the optimized geometries with the CCSD method with a QRHF reference[47] are 1.789 and 1.684 Å, and 132.1°, for $R_{B-Cl}$, $R_{B-Cl'}$, and $\angle_{ClBCl'}$, respectively, in the $C_{2v}$ symmetry and $R_{B-Cl}$ is 1.739 Å in $D_{3h}$ symmetry. The $\Delta G_0$ calculated as the difference in the QRHF-CCSD(T)[47] total energy at the QRHF-CCSD geometry is reduced to 0.17 eV, but the $C_{2v}$(2L1S) structure is still the lowest state. Even though the 2L1S state of $BCl_3^+$ is the lowest state in the present calculation, it is possible, indeed likely, that the $^2A_2'$ state in $D_{3h}$ symmetry is the true ground state, as could be shown in a more definitive study. The other two states, $^2B_1$ and $^2B_2$, would then likely be transition states for pseudorotation of the ground state.

The bond length of $BCl_3$ can be directly compared with the experimental value[65] and shows good agreement. Because the experimental bond lengths for the $BCl_3^+$ and the $BCl_3^-$ ion have not been previously reported, no direct comparison to experiment is possible.

The vertical ionization potential (VIP), adiabatic ionization potential (AIP), vertical electron affinity (VEA), adiabatic electron affinity (AEA), and the vertical electron detachment energy (VEDE) are calculated as the difference between CCSD(T) energies at the MBPT(2) geometries. The calculated VIP and AIP in Table VI show good agreement with the results from the photoionization study.[71] The calculated adiabatic electron affinity (AEA), 0.30 eV–0.40 eV with CCSD and CCSD(T), also shows good agreement with the experimental value, $0.33 \pm 0.2$ eV.[37]

Though the negative ion, $BCl_3^-$, is directly detected from the charge transfer reaction,[37] it was not directly detected in the electron collision experiment. The negative value of VEA and positive value of AEA means that there may be some threshold in the formation of negative ions by electron attachment. The value of the VEA can be compared with the earlier experimental result that the cross section for negative ion production from $BCl_3$ by low-energy electron attachment shows a maximum near 0.4 eV.[21] Therefore the large anion currents resulting from electron attachment to $BCl_3$ at energies less than 0.5 eV is the result of the formation of $BCl_3^-$.

The VEDE can be compared with the optogalvanic signal of the photodetachment process at 1.77 eV.[67] The calculated vertical electron detachment energy of $Cl_2^-$ with CCSD//MBPT(2) is 3.69 eV (experimental value, 3.61 eV) and that of $BCl_2^-(X^1A_1)$ is 1.11 eV. $BCl^-$ is less stable than BCl. In other words, the calculated value of the VEDE supports the previous interpretation of the optogalvanic signal as a photodetachment of $BCl_3^-$ rather than another chemical species. While the singlet state of $BCl_2^-$ is stable relative to $BCl_2$, both vertically and adiabatically, $BCl_3^-$ is stable only adiabatically.

Relations between VEA, AEA, and VDEA to some points on the potential energy surfaces are described in Fig. 1.

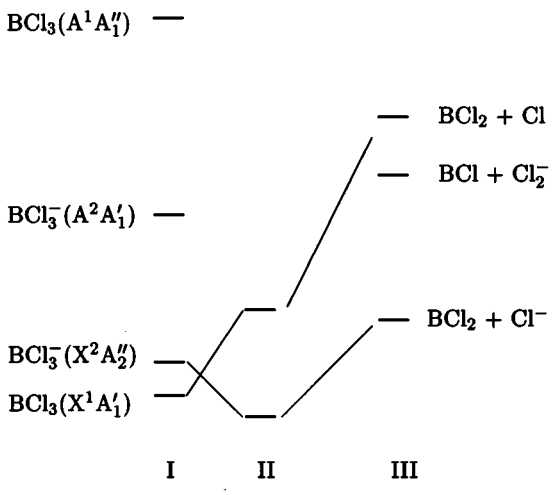


FIG. 1. Relations of VEA, AEA, and VDEA to some points of the potential energy surface. The stability of the first two states of $BCl_3$ and $BCl_3^-$ relative to their fragments. I—at $BCl_3$ geometry in $D_{3h}$ symmetry; II—at $BCl_3^-$ geometry in $C_{3v}$ symmetry; III—single bond breaking limit.

The vibrational frequencies of $BCl_3$ and $BCl_3^-$ are obtained from a Hessian calculated by two-sided numerical differentiation using analytically calculated MBPT(2) gradients. The calculated values for $BCl_3$ in Table VII show reasonable agreement with the experimental values obtained by IR and Raman spectra.[68] The fundamental transitions in the IR spectra, however, are mainly determined not by the whole molecule but by some portion of the molecule. The calculated value for the IR frequency of $BCl_3^-$ can be compared with the recent experiment of Jacox *et al.*[26] for $\nu_3$, and indirectly with some IR peaks of molecules, such as $CH_3CN \cdot BCl_3$. The latter is regarded as an electron donor–acceptor complex providing some estimate of the vibrations of the $BCl_3$ part. Based on the fact that the calculated value for the frequency of IR peaks is 2–5% larger than the experimental value, as in the $BCl_3$ case, the actual position of IR peaks of $BCl_3^-$ can be anticipated from the calculated values.

The order of molecular oritals, orbital energies ($\varepsilon$), and vertical ionization potentials (IP) are given in Table VIII.

TABLE VII. Frequencies of vibrational excitations in $BCl_3$ and $BCl_3^-$, calculated with the MBPT(2) method (in $cm^{-1}$).

| $BCl_3$ | $\nu_1(A_1')$ | $\nu_2(A_2'')$ | $\nu_3(E')$ | $\nu_4(E')$ |
|---|---|---|---|---|
| Basis-I | 480 | 462 | 987 | 257 |
| Basis-II | 488 | 470 | 1005 | 263 |
| Expt.[a] | 471 | 462 | 958 | 243 |
| $BCl_3^-$ | $\nu_1(A_1)$ | $\nu_2(A_1)$ | $\nu_3(E)$ | $\nu_4(E)$ |
| Basis-I | 551 | 315 | 695 | 214 |
| Basis-II | 550 | 324 | 712 | 222 |
| Expt.[b,c] | | | 686 | |

[a]Experimental values from IR and Raman Spectra (Ref. 68).
[b]Experiments of Jacox *et al.* for $BCl_3^-$ (Ref. 26).
[c]Observed IR frequencies of $CH_3CN \cdot BCl_3$ (Ref. 69) corresponding to vibrations of the $BCl_3$ part are 411, 287, 746, and ~220 $cm^{-1}$, respectively.

Vertical ionization potentials of each molecular orbital are calculated by the IP-EOM-CCSD method.[70,30] The first IP of $BCl_3$ by the IP-EOM-CCSD is 0.10 eV lower than that obtained by the CCSD energy difference in Table VI. The results in Table VIII show fairly good agreement, within 1% with the experimental values obtained by photoelectron spectroscopy for $BCl_3$.[71] Because of the open-shell electronic configuration of $BCl_3^-$, the vertical ionization potential calculated by the IP-EOM-CCSD method with a UHF reference shows two values for each molecular orbital. Average values are given in the table. This calculated value might be helpful for the detection of experimental signals in the future. Because of the negative charge, the ionization potential of an MO in $BCl_3^-$ is only about half of the corresponding MO in $BCl_3$.

## VI. EXCITED STATES OF $BCl_3$

Only optically allowed electronic states of $BCl_3$ have been studied by vacuum UV spectroscopy.[24,72] The first excitation was assigned[72] as the transition of $3a_2'' \leftarrow 2e''(^1E' \leftarrow {}^1A_1')$, and the second excitation is guessed to be $7a_1' \leftarrow 7e'(^1E' \leftarrow {}^1A_1')$ or $8e' \leftarrow 2a_2'(^1E' \leftarrow {}^1A_1')$. Using the largest transition amplitude calculated by EOM calculations,[32] whole assignments, not only for optically allowed but for optically forbidden transitions, are given in Table IX along with the excitation energies and oscillator strengths. From the calculated result, the second band is assigned as the $7a_1' \leftarrow 7e'$ transition and the third to $8e' \leftarrow 2e_2''$. The effect of the vibrational energy levels is not considered in the calculated electronic excitation energies, and experimental values are converted simply from the $\lambda_{max}$ of UV absorption bands. Although the agreement between the two values cannot be perfect, the calculated results are adequate for qualitative analysis and predictions of the UV spectrum. Compared with the experimental results with the above considerations, the calculated results in Table IX are expected to be reasonable, typically within ~0.3 eV for low-lying valence states and Rydberg states. For the latter, additional Rydberg basis functions would be required to recover the error.

Through vibronically allowed transitions, three optically forbidden transitions between the first and the second optically allowed transitions are likely to make a contribution to the broad shoulder observed between the two strong bands. The third band is expected to be weak, which contrasts with the vacuum UV spectrum of $BBr_3$.

In the case of Penning ionization followed by dissociative electron recombination, the initial positive ion, $BCl_3^+$, is most likely to be formed by the removal of the electron from the HOMO, $2a_2'$. Therefore, the excited states of $BCl_3$ by electron recombination after Penning ionization by Ar* can be expected to have one hole in the $2a_2'$ orbital and one electron in the unoccupied molecular orbitals of $BCl_3$. Selection rules for optical activity play no role in this case. Not only singlet states but triplet states can be formed by electron recombination. Excitation energies to these triplet states are also given with the corresponding singlet states. Among the

TABLE VIII. Ordering of molecular orbitals and vertical ionization potentials (IP) calculated by IP-EOM–CCSD for $BCl_3$ and $BCl_3^-$.

| $BCl_3, X^1A_1', D_{3h}$ | | | | | $BCl_3^-, X^2A_1, C_{3v}$ | | | | |
|---|---|---|---|---|---|---|---|---|---|
| | $\varepsilon$[a] | IP | | | IP | | $\varepsilon$[a](eV) | | |
| Orbital | (eV) | Basis-I | Basis-II | Expt.[b] | Basis-I | Basis-II | $\alpha$ | $\beta$ | Orbital |
| $6a_1'$ | −19.13 | 17.79 | 17.61 | 17.70,17.74 | | | −13.38 | −12.49 | $7a_1$ |
| $6e'$ | −16.85 | 15.50 | 15.67 | 15.51,15.54 | | | −10.19 | −9.96 | $7e$ |
| $2a_2''$ | −15.40 | 14.22 | 14.50 | 14.41,14.42 | 7.66 | 7.91 | −9.68 | −8.67 | $8a_1$ |
| $7e'$ | −13.76 | 12.50 | 12.78 | 12.75,12.66 | 6.70 | 6.95 | −8.13 | −7.91 | $8e$ |
| $8e''$ | −13.49 | 12.30 | 12.57 | 12.65,12.39 | 6.10 | 6.36 | −7.41 | −7.31 | $9e$ |
| $2a_2'$ | −12.81 | 11.56 | 11.84 | 11.82,11.73 | 5.72 | 5.97 | −7.00 | −6.97 | $2a_2$ |
| $3a_2''$ | 1.84 | | | | 1.92 | 2.00 | −3.33 | 8.38 | $9a_1$ |
| $7a_1'$ | 4.36 | | | | | | 8.88 | 9.03 | $10a_1$ |
| $8e'$ | 4.83 | | | | | | 9.02 | 9.22 | $10e$ |
| $4a_2''$ | 5.99 | | | | | | 10.87 | 10.98 | $11a_1$ |
| $9e'$ | 6.34 | | | | | | 11.03 | 11.12 | $11e$ |

[a]Koopmans' value for the IP is the negative of the orbital energy.
[b]Experimental values from photoelectron spectroscopy of Refs. 24 and 71, respectively.

many excited states in Table IX, only the states formed by electron excitation from $2a_2'$ are meaningful in the dissociative recombination process after the Penning ionization. These states are designated as the dissociation-path in Table IX, because only these states are expected to be involved in the dissociative electron recombination to $BCl_3^+$.

## VII. FLUORESCENCE SPECTRA

Some possible photodissociation processes of $BCl_3$ through excited states have been studied by absorption and fluorescence spectroscopy in the vacuum UV region.[23,24] Understanding this fluorescence spectra is an important but difficult goal for theory. Fluorescence is a dynamical process that can occur from intermediate geometries of the excited states. It appears that four optically allowed transitions are observed and studied in the experiment resulting in bands termed A, B, C, and D while the first three excited states of $BCl_3$ decompose into $BCl_2$ and Cl fragments according to the experiment, the fourth excited state decays into BCl and 2Cl. To become oriented, consider Figs. 2 and 3 where the transition energies for the four bands are shown with the corresponding energy levels for $BCl_3$ and its fragments, at the various optimum geometries.

The ground state of $BCl_2$ has a $\sim 2b_1^2 2a_2^2 7b_2^2 8a_1^1$ electronic configuration. The EOM-CCSD method with a UHF reference function is reasonable for doublet open-shell cases, providing some excited states of $BCl_2$. The first excitation corresponds to the electron transition from the HOMO of $BCl_2$ ($a_1$) to the LUMO ($b_1$). The excitation energy of this transition, $A^2B_1 \leftarrow X^2A_1$, is calculated to be 2.51 eV. Be-

TABLE IX. Electronic vertical excitation energies of $BCl_3$ calculated by EOM-CCSD with Basis-I.

| Electronic state | $(T_e')$[a] (in eV) Triplet | Singlet | $f_{osc}$[b] | Transition | Optical activity | Dissociative path[c] |
|---|---|---|---|---|---|---|
| $A_1'$ | 0.00 | 0.00 | | | | |
| $A_1''$ | 6.27 | 6.35 | 0.0 | $3a_2'' \leftarrow 2a_2'$ | | active |
| $E''$ | 7.10 | 7.21 | 0.0 | $3a_2'' \leftarrow 7e'$ | | |
| $E'$ | 6.77 | 7.48 (7.20)[d] (7.17)[e] | 0.199 | $3a_2'' \leftarrow 2e''$ | allowed | |
| $A_2'$ | 8.50 | 9.06 | 0.0 | $7a_1' \leftarrow 2a_2'$ | | active |
| $A_1'$ | 8.18 | 9.48 | 0.0 | $3a_2'' \leftarrow 2a_2''$ | | |
| $E''$ | 9.13 | 9.62 | 0.0 | $3a_2'' \leftarrow 6e'$ | | |
| $E'$ | 9.12 | 9.89 (9.20)[d] (9.80)[e] | 0.202 | $7a_1' \leftarrow 7e'$ | allowed | |
| $E''$ | 9.64 | 10.11 | 0.0 | $3a_2'' \leftarrow 6e'$ | | |
| $E'$ | 10.66 | 10.75 (10.31)[e] | 0.080 | $8e' \leftarrow 2e''$ | allowed | |

[a]Vertical excitation energy at $BCl_3$ geometry.
[b]Oscillator strength calculated by the dipole length approximation (Ref. 32).
[c]The excited state formed without coexcitation when the ground state of $BCl_3^+$ recombines with an electron.
[d]The $\lambda_{max}$ of the UV spectra ranges from 200 to 120 nm (Ref. 72).
[e]From the threshold of the absorption and fluorescence spectroscopy of $BCl_3$ (Ref. 23).

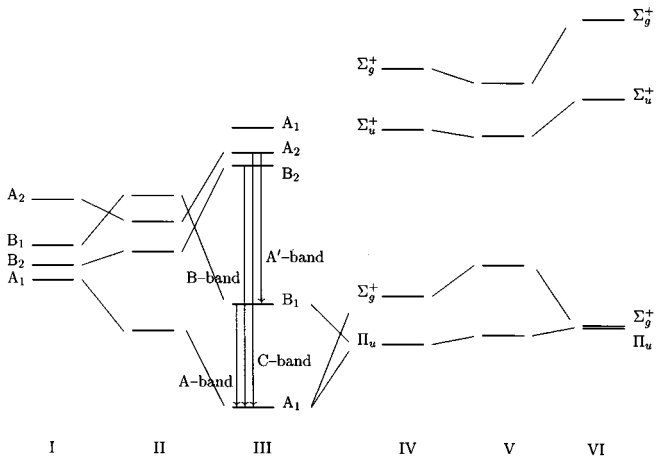


FIG. 2. Correlation diagram between excited states of Table XI at optimized geometries for the $^2B_2$ state (I), $^2A_2$ state (II), $^2A_1$ state (III), $^2\Pi_u(^2B_1)$ state (IV), $^2\Sigma_u^-$ state (V), and $^2\Sigma_g^+$ state (VI), on the potential surface of $BCl_2$.

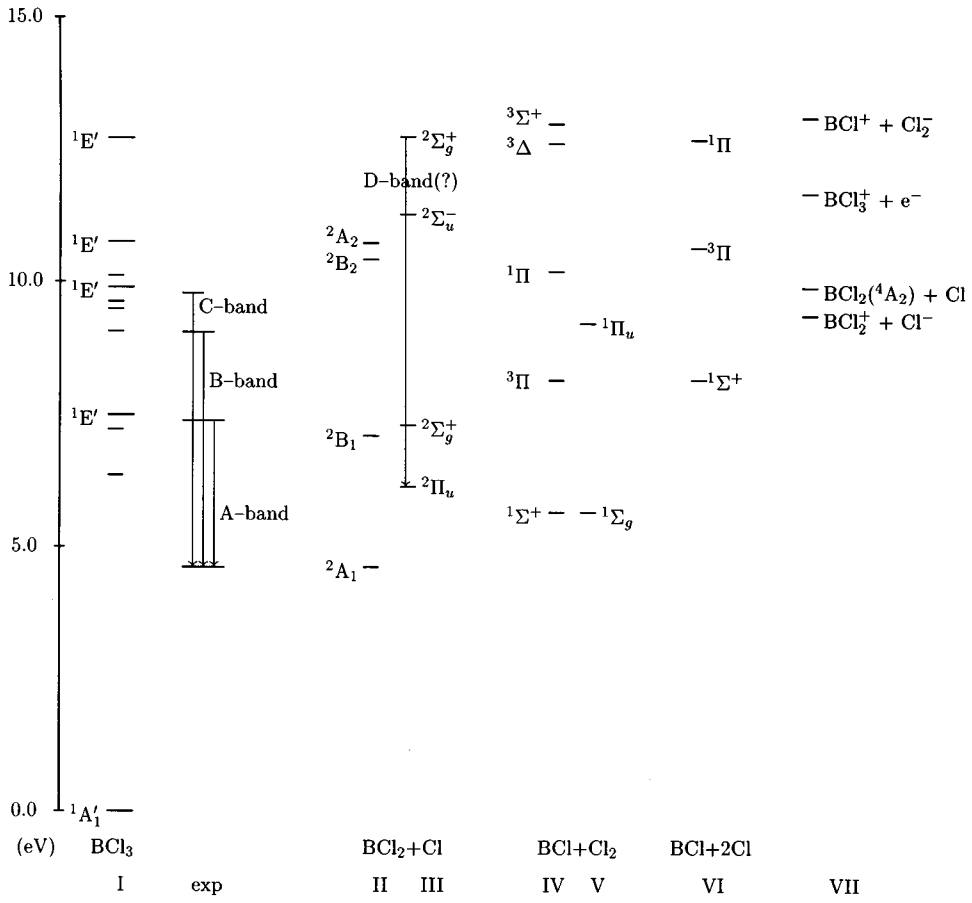


FIG. 3. Energy diagram for fragments from $BCl_3$. Transition energies for A, B, C, and D bands are shown for reference. I—Singlet states of $BCl_3$; exp—energy levels suggested by the experiments (Ref. 23); II—doublet states of $BCl_2$ in a $C_{2v}$ structure; III—doublet states of $BCl_2$ in $D_{\infty h}$; IV—singlet and triplet states of BCl; V—singlet states of $Cl_2$; VI—singlet and triplet states of BCl; VII—other fragments.

cause the symmetry of the first excited state differs from the ground state, the excitation energy is also calculated as the difference in the total CCSD(T) energies between two states with different electronic configurations, and the result is 2.48 eV. This result can be compared with the A-band of the experimental result. The short wavelength end (the origin) of the A-band occurs at 450 nm (2.76 eV) and $\lambda_{max}$ is around 500 nm (2.48 eV). The coincidence with the computed vertical transitions strongly support assigning the A-band to this deexcitation.

TABLE X. Experimental results of the fluorescences from the photoexcitation of $BCl_3$. Experimental data from Refs. 23 and 56 are collected in this table.

| $\lambda$(UV)[a] | Band | $\lambda$(Flu)[b] | Up-limit[c] | $\lambda(I_{max})$[d] |
|---|---|---|---|---|
| 7.17 | A | 2.76 | 2.56 | 2.47 |
| 9.80 | B | 4.43 | 5.19 | 3.44 |
| 10.31 | A′ and C | 5.17 | 5.70 | 4.10 |
| 12.72 | D | 6.20 | | |

[a]Threshold UV energy to produce the fluorescence band.
[b]The short wavelength-end of the band.
[c]The upper limit for the potential energy; see the text.
[d]$\lambda$ at maximum fluorescence intensity, guessed from spectroscopic graphs.

The experimental result[23] considers three more excited states in $BCl_2$ which are assigned to the B-, C-, and D-bands. Here the differences in energy between the origin and $\lambda_{max}$ are much greater. The short wavelength ends of these three bands occur at 280 nm (4.43 eV), 240 nm (5.17 eV), and 200 nm (6.20 ev). These experimental results are summarized in Table X and Figs. 2 and 3. The vertical transition energy for the optically allowed excited states of $BCl_3$, are given in Table IX and Fig. 3.

According to the calculated results of the present study, given in Table XI, the next two excited states, $^2B_2$ and $^2A_2$ of $BCl_2$ at the optimized geometry of the ground state fall at 5.81 eV and 6.12 eV above the ground state, with the errors of the present calculations estimated to be high by up to $\sim$0.3 eV.

The $^2B_2$ state has a $\sim 2b_1^2 2a_2^2 7b_2^1 8a_1^2$ electronic configuration and the $^2A_2$ state a $\sim 2b_1^2 2a_2^1 7b_2^2 8a_1^2$ electronic configuration. In contrast to the $BF_2$ case where the second excited state has Rydberg character, because the state is made by the excitation of the HOMO electron into a virtual MO, the second and the third excited states of $BCl_2$ can be regarded as valence states because the electronic configuration of these two excited states are the result of electron

TABLE XI. Vertical excitation energies (in eV) of $BCl_2$ calculated as the difference in CCSD(T) energies at selected geometries. Four fluorescence bands[23,56] start at 2.76 (A-), 4.43(B-), 5.17(C-), and 6.20 eV (D-band), respectively. The geometries correspond to those in Fig. 2.

| Geometry | | I | II | III | III′ | | IV | V | VI |
|---|---|---|---|---|---|---|---|---|---|
| $R_e$[a] | | 2.010 | 2.039 | 1.746 | 1.720 | | 1.717 | 1.638 | 1.858 |
| ∠[b] | | 77.5 | 92.3 | 124.6 | 125.1 | | 180.0 | 180.0 | 180.0 |
| $\Delta H^{oc}$ | | 3.07 | 1.84 | 0.00 | | | 1.52 | 1.74 | 1.92 |
| | $A_1$ | 0.00 | 0.00 | 0.00 | | $\Pi_u$ | 0.00 | 0.00 | 0.00 |
| | $B_1$ | 0.83 | 3.25 | 2.48 | | $\Sigma_g^+$ | 1.16 | 1.69 | 0.06 |
| | | | | (2.40)[d] | (2.35)[d] | | | | |
| | | | | (2.48)[e] | | | | | |
| | $B_2$ | 0.35 | 1.90 | 5.81 | | $\Sigma_u^+$ | 5.15 | 4.79 | 5.50 |
| | | | | (5.90)[d] | (5.88)[d] | | | | |
| | | | | (5.71)[e] | | | | | |
| | $A_2$ | 1.93 | 2.62 | 6.12 | | $(\Sigma_g^+)$[f] | 6.62 | 6.06 | 7.41 |
| | | | | (6.20)[d] | | | | | |
| | | | | (6.02)[e] | | | | | |
| | $(A_1)$[f] | | | 6.72 | | | | | |
| | … | | | | | | … | | |
| | | | | | | | $(\Delta_u)$[f] | 12.61 | |

[a]B–Cl bond length in Å.
[b]∠ Cl–B–Cl in degrees.
[c]Energy difference (in eV) from the global minimum, III.
[d]Result with the PVTZ (Ref. 43) all-electron basis sets of the B and the Cl atom. All electrons are correlated.
[e]Results with the ghost atom having a PVDZ basis set on the B atom; see the text.
[f]Excitation energies of these states are calculated by the EOM-CCSD method.

redistributions among the valence orbitals. The difference in orbital energies between the HOMO and the next occupied MO is about 3.0 eV in $BCl_2$, while it is about 7.0 eV in $BF_2$. Because the change in the electronic configuration from the ground state into these two excited states involves the movement of two electrons, one excitation and one deexcitation, the EOM-CCSD method restricted to double excitations is probably not adequate. (Triples largely correct this problem.[73]) Thus, the excitation energies of these two states are also calculated as the difference between CCSD(T) energies at the MBPT(2) geometry. Other excited states caused by the excitation of the HOMO electron into virtual orbitals turn out to have much higher energies.

In order to check the effect of the size of the basis sets, the same kind of calculations are performed at the same geometry with all-electron PVTZ basis sets on the B and the Cl atom. All electrons are correlated at the post-HF calculations. As given in the parenthesis in Table XI, the effect of the basis set size is only about 0.1 eV. These values are changed less than 0.1 eV even by another calculation with the ghost atom having the same PVDZ basis set of the B atom and locating 0.873 Å (half of the B–Cl bond length) away from the B atom along the $C_{2v}$ axis. The geometry is also optimized with the PVTZ basis set and the MBPT(2) method (the III′ in Table XI) and the excitation energies are calculated in the same way as differences in the CCSD(T) energies. The change in the excitation energies is still only about 0.1 eV.

To offer some insight about the potential surface of each excited state, some points over the whole potential surface are selected (see Table XI and Fig. 3). The optimized bond length and bond angle in $C_{2v}$ symmetry of the $^2B_2$ state, geometry-I, are 2.010 Å and 77.5°, and those of the $^2A_2$ state, geometry-II, are 2.039 Å and 92.3°. Even at these geometries, the lowest state is the $^2A_1$ state, which is 3.07 eV (at the geometry-I) and 1.84 eV (at the geometry-II) higher than the global minimum, geometry-III. The order of the other excited states, however, are interchanged.

When the geometry of the $B_1$ state is optimized, its symmetry is converted from $C_{2v}$ into the linear structure, geometry-IV. The optimized bond length in the linear structure, $D_{\infty h}$ symmetry, is 1.717 Å, and the total energy of the ground state, $^2\Pi$, in this structure is 0.35 eV higher than the global minimum state, $^2A_1$. The excitation energies for the first and the second excited states in the linear structure are calculated as the difference in the CCSD(T) total energy from that of the ground state. The excitation energy for the third excited state in the linear structure is calculated with the EOM-CCSD method. Total energies of the four states are obtained also at the optimized bond length of the $^2\Sigma_u^+$ state (geometry-V, 1.638 Å) and that of the $^2\Sigma_g^+$ state (geometry-VI, 1.858 Å).

To attempt to offer more conclusive numerical results, we would have to obtain the whole potential energy surface and study the vibrations and the Frank–Condon factors for all possible vibronic transitions, as was performed for $BF_2$.[74] For our present purposes, we offer a qualitative analysis based on the results for six points selected from the potential surface. All these results are shown in Table XI and Fig. 2. If the photofragmentation produces $BCl_2$ in its second excited state in the linear structure, $\Sigma_u^+$ the decay into $\Sigma_g^+$ is allowed through E1 (electric dipole transition) with the transition energy ranging from 3.10 eV to 5.40 eV. Transition to

$\Pi_u$ is allowed through E2 (electric quadrupole transition) and M1 (magnetic dipole transition), and the transition energy may be around 5.0 eV. The third excited state, $\Sigma_g^+$, either decays into $\Pi_u$ through an E1 transition or decays into $\Sigma_g^+$ through an E2 transition. The transition energies are around 6.5 eV for the E1 transition and 4.5 eV for the E2 transition. Though the deexcitation from the second and the third excited states of $BCl_2$ in the linear structure can be a candidate for the B- and C-bands, the energetic relations shown in Fig. 3 preclude this as these states cannot be obtained from the second and the third excited state of $BCl_3$. The $\Delta G_0$ between $BCl_3$ and ($BCl_2$,$^2A_1$,$C_{2v}$+Cl,$^2P$) is observed to be 4.61 eV,[52,75] while the computed value obtained as the difference in CCSD(T) total energies at MBPT(2) geometries with Basis-I is 4.76 eV after the zero-point correction. Because the $X^2\Pi_u$ state of $BCl_2$ in the linear structure falls 1.52 eV higher than the $X^2A_1$ of $BCl_2$ in the $C_{2v}$ structure, the $\Delta G_0$ between $X^1A_1'$ of $BCl_3$ and ($X^2\Pi_u$, $BCl_2$+$^2$P,Cl) is 6.13 eV. ($\Delta G_0$ for $BCl_3 \rightarrow Cl_2$+Cl is taken as 4.61 eV, here and in Fig. 3.) Considering the transition energy between $^2\Sigma_u^-$ and $^2\Pi_u$ of $BCl_2$, 5.15 eV, the threshold energy to make the second excited state, $^2\Sigma_u^-$ of $BCl_2$ in $D_{\infty h}$ from the excited states of $BCl_3$, is 11.28 eV. The threshold energy for the $^2\Sigma_g^+$ state is calculated to be 12.75 eV in the same way. Even if the error in the present calculations for excited states were as large as 1.0 eV, it is hard to see how the $^2\Sigma_u^-$ and $^2\Sigma_g^+$ states can be attained from the second and the third optically allowed excited states of $BCl_3$, because the excitation energies are 9.80 and 10.31 eV, respectively. Figure 3 shows the energetic relations among all possible electronic states of the fragments. All electronic states are shown relative to the ground state of $BCl_3$ with a proportional energy scale.

From the features of the potential surface, schematically shown in Fig. 2 and discussed above, we can unambiguously identify the first excited state in $C_{2v}$ symmetry, $^2B_1$, as the state which produces the first fluorescence band, designated as the A-band in Ref. 23.

Next, although the vertical transition energy between the ground $^2A_1$ state and the $^2B_2$ state at the geometry III of Fig. 2, 5.81 eV, differs substantially from the short wavelength end of the B-band, the $^2B_2$ state can still be responsible for the B-band because unlike the $B_1$ state, this state has a long enough lifetime ($\sim 10^{-9}$ s), to imply a substantial geometric change before fluorescence. The latter can occur an order of magnitude faster. At the optimized geometry of the $^2B_2$ excited state (the geometry I of Fig. 2), the vertical deexcitation energy is computed to be only 0.35 eV. Consequently, the most we can say is that the experimental value should fall between 0.35 and 5.86 eV, as it does at 4.43 eV. Based on the same argument and a similar long life time,[23] the $^2A_2$ state can be responsible for the C-band because the deexcitation energies at geometries II and III of Fig. 2 and Table XI fall between 2.62 and 6.12 eV, correspoding to the 5.17 observed. To do better would require a detailed dynamical treatment.

Though pure electronic transitions between $A_1$ and $A_2$ states are forbidden, the coupling with the nuclear vibrational mode makes vibronic transitions possible either between the $b_2$ mode of the $A_2$ state and the $a_1$ mode of the $A_1$ state; or between the $a_1$ mode of the $A_2$ state and the $b_2$ mode of the $A_1$ state. On the other hand, the transition from the third excited state to the first excited state, which is an optically allowed transition, might be the source of another weak $A'$-band which is observed when the excitation UV energy is larger than 10.3 eV. Three vertical arrows at the second column (exp) in Fig. 3 represent the suggested energy levels for the experiment.[23] The energy level of the $B_2$ state at geometry-I of Fig. 2 and the energy level of the $A_2$ state at geometry-II of Fig. 2 are presented in columns II and III of Fig. 3 as well as their energy levels at geometry-III of Fig. 2.

While the earlier fluorescence result[23] differentiates the B- and C-bands, they are not clearly distingushed in the later experiments.[24]

The third excitation energy in $D_{\infty h}$ symmetry (geometry-IV,V,VI), in Table XI and Fig. 2 can be compared with the D-band, 200–260 nm (6.20–4.77 eV),[56] of the fluorescence spectrum. The third excited state, $\Sigma_g^+$, in the linear structure can be reached by a threshold energy of 12.72 eV, and might be the source of the D-band.

Even though the $^2B_2$ and $^2A_2$ states are considered to be the source of the B- and C-bands, respectively, other possibilities cannot be completely eliminated.

We also consider the possibility of transitions between quartet states. The lowest quartet state of $BCl_2$, $^4A_2$, is located at an energy 5.3 eV higher than the $X^2A_1$ state of $BCl_2$ and 9.9 eV above the $X^1A_1'$ state of $BCl_3$. In order for the excited quartet states to be the source of the B- and the C-bands, the excited quartet states must have at least 9.73 eV and 10.47 eV excess energy relative to the $X^2A_1$ state of $BCl_2$. Therefore, the threshold energy required to obtain such excited quartet states from $BCl_3$ would be 14.34 eV and 15.08 eV, respectively. Therefore, these excited quartet states cannot be formed from the second and the third optically allowed excited states of $BCl_3$. These energetic rela-

TABLE XII. Geometries and electronic excitation energies of $B_2Cl_4$ systems. Geometries are optimized by the MBPT(2) method with the Basis-I. The lowest excitation energies are calculated by EA-EOM-CCSD method[34] at the MBPT(2) geometry.

| | $X^1A_1, D_{2d}$ $\sim 7b_2^2, 2b_1^2, 2a_2^2, 10e^4, 8a_1^2$ | | | $a^3B_{1u}, D_{3h}$ $\sim 2b_{1u}^2, 2b_{3g}^2, 7_{3u}^2, 8b_{2u}^2, 2b_{2g}^2$ $2a_u^2, 7b_{1g}^2, 3b_{1u}^1, 9a_g^1$ | | |
|---|---|---|---|---|---|---|
| $R_{B--B}$ (Å) | 1.696 | | | 1.776 | | |
| $R_{B--Cl}$ (Å) | 1.759 | | | 1.750 | | |
| $\angle_{ClBB}$ (°) | 120.1 | | | 116.5 | | |
| $\tau$[a] | 90.0 | | | 0.0 | | |
| $D_e$ (eV)[b] | 4.30 | | | 0.66 | | |
| $D_e$ (eV)[c] | 2.53 | | | −1.11 | | |
| | | $T_e$(eV)[d] | $f$[e] | | $T_e$(eV)[d] | $f$[e] |
| | $8a_1 \rightarrow 11e$ | 5.48 | 0.005 | $b_{1g} \rightarrow b_{1u}$ | 1.80 | 0.0 |

[a]Torsional angle between Cl–B–B–Cl.
[b]Dissociation energy into $BCl_2$+$BCl_2$.
[c]Dissociation energy into $BCl_3$+BCl.
[d]Vertical excitation energies by the EA-EOM-CCSD method (Ref. 34).
[e]Calculated oscillator strength (Ref. 32).

tions are also shown in column VII of Fig. 3.

The absence of the prominent signal of 4.557 eV from the $^1\Pi \rightarrow {}^1\Sigma$ transition of BCl was the main reason to draw the conclusion that the B- and C-bands stem from excited states of the $BCl_2$ fragment. However, since $(BCl+Cl_2)^*$ is another possible product complex, other possibilities might be considered. The energetic relations in these cases are shown in columns IV and V of Fig. 3. If the initial excited state of BCl is a highly excited triplet state, it can decay into the lowest triplet state $(a^3\Pi)$. The transition energies between these triplet states are 4.48 eV and 4.85 eV for the $a^3\Pi \leftarrow b^3\Sigma^+(\Delta)$ and $a^3\Pi \leftarrow c^3\Delta(\Sigma^+)$, respectively. It should also be noticed that the excitation energy to the first excited state, $^1\Pi_u$, of the $Cl_2$ molecule is about 3.57 eV. That can be compared with the unusually large peak at 3.44 eV in the fluorescence spectrum. This $Cl_2$ state is attainable from the second optically allowed excited state of $BCl_3$. The $^1\Pi_u$ state of $Cl_2$, however, dissociates into two Cl atoms. Because the $\Delta G_0$ between the $X^1A_1$ state of $BCl_3$ and $(X^1\Sigma^+, BCl + X^1\Sigma_g, Cl_2)$ is 5.61 eV[52,75] (computed value by the Basis-I is 6.01 eV) and the $a^3\Pi$ state falls 2.54 eV higher than that, the minimum threshold energy to make the $b^3\Sigma^+$ state of BCl from the $BCl_3$ ground state is 12.63 eV. The threshold energy to produce the $c^3\Delta(\Sigma^+)$ is 13.00 eV, in the same way. However, the B- and C-bands are observed with a threshold energy of 9.80 eV and 10.31 eV, respectively.[23] Moreover, all these three excited states, $^3\Delta$ and $^3\Sigma^+$ of BCl and $^1\Pi_u$ of $Cl_2$, are dissociative states which cannot be the source of a fluorescence spectrum. It also should be mentioned that the first and the second excitation energies of $BCl^+$ are calculated to be 4.55 eV for $A^2\Pi$ and 5.36 eV for $B^2\Pi$. These values are very close to the short wavelength ends of the B- and the C-bands. The threshold energy to make the product $BCl^+ + Cl_2^-$, however, is about 13.06 eV, and these two excited states of $BCl^+$ are again dissociative states.

Almost the same intensities of the B- and C-bands as the A-bands in the fluorescence spectrum exclude the possibilities of other electronic transitions within molecular systems which can be formed by secondary reactions like radical recombination. The $B_2Cl_4$ molecule is one of the best known and most probable products of such secondary reactions. The structure of $X^1A_g$ and $a^3B_{1u}$ states of $B_2Cl_4$ are optimized by MBPT(2) with Basis-I. While the triplet state has $D_{2h}$ symmetry, the singlet state has $D_{2d}$ symmetry, the same as earlier experimental results.[76] The results in Table XII also show the transition energies for low-lying excited states. These electronic transition energies are calculated by the EA-EOMCC method.[34]

The dissociation energies of the $X^1A_1$ state of $B_2Cl_4$ are calculated as the difference of CCSD total energies at MBPT(2) geometries with Basis-I. The calculated dissociation energies into $2BCl_2$ and $BCl_3+BCl$ are 4.30 eV and 3.64 eV, respectively. Because the triplet state falls 3.64 eV higher than the singlet state, the dissociation energies of the $a^3B_{1u}$ state of $B_2Cl_4$ are 0.66 eV for $2BCl_2$ and $-1.11$ eV for $BCl_3+BCl$. The triplet state is unstable relative to dissociation into $BCl_3$ and BCl, which might relate to the well-known phenomena[77] that gaseous $B_2Cl_4$ spontaneously decomposes into $BCl_3$ and BCl at room temperature.

The transition energy, 5.48 eV, into the first excited singlet state is close to the C-band, 5.17 eV, but the oscillator strength is very small and the excitation energy is larger than the dissociation energies. Though the possibility cannot be completely eliminated, it is hard to believe that $B_2Cl_4$ is responsible for the C-bands.

## VIII. OTHER DECOMPOSITION PATHWAYS OF $BCl_3$

According to the recent experimental study,[75] the threshold energy in the electron collision study for the formation of $BCl_2$ and Cl from $BCl_3$ was 4.61 eV. The threshold energy for the formation of BCl and $Cl_2$ is 5.65. When these threshold energies are compared with the excitation energies of $BCl_3$, it is quite clear that the excited states of $BCl_3$ cannot be involved in the above process. Because the ionization potentials of $BCl_3$ are higher than 11 eV and the first excitation energy of $BCl_3$ is about 6.3 eV, electronic states of $BCl_3^-$ can only form by electron attachment transition states in the decomposition process of $BCl_3$ into fragments in such low-energy collisions.

According to the present study, the decomposition path of the ground state of $BCl_3^-$ shows no potential barrier decomposition into $BCl_2$ and $Cl^-$, and the dissociation energy is 1.98 eV at the CCSD level with Basis-I. The electron affinity of Cl with this basis set was underestimated by about 0.45 eV. The zero-point energies of $BCl_2$, $BCl_3$, and $BCl_3^-$ are 0.13 eV, 0.22 eV, and 0.17 eV, respectively, and the adiabatic EA of $BCl_3$ is 0.30 eV. Considering all these things, the dissociation energy of $BCl_3^-$ into $BCl_2$ and $Cl^-$ is estimated to be around 1.59 eV, and the threshold energy to make the $Cl^-$ ion from $BCl_3$ becomes about 1.11 eV, which explains many early experimental results that the excitation caused by dissociative electron attachment by beam experiments shows a peak at 1.1 eV.[21]

The dissociation energy for the reaction $BCl_3^- \rightarrow BCl + Cl_2^-$ is calculated as the difference between the CCSD(T) energies at the MBPT(2) geometries. Because the electron affinity of $Cl_2$ is overestimated by 0.08 eV with the same basis set, the calculated dissociation energy, 3.93 eV, is corrected to 4.01 eV. The dissociation energies of $BCl_3^- \rightarrow BCl + Cl + Cl^-$ is calculated as 5.00 eV. Considering the underestimation of the electron affinity of Cl, the dissociation energy is estimated to be about 4.55 eV.

As shown in Table VI and Fig. 1, the ground state of $BCl_3^-$, $X^2A_2''$ in $D_{3h}$ ($X^2A_1$ in $C_{3v}$), at the $BCl_3$ geometry is unstable relative to neutral $BCl_3$ and a free electron, but stable relative to dissociation into $BCl_2$ and $Cl^-$. Possible relations to other fragments are discussed above. The next electronic state of $BCl_3^-$ is calculated by the electron-attachment equation-of-motion (EA-EOMCC) method.[34] The excitation energy from the $X^2A_2''$ state to this state, $A^2A_1'$ in $D_{3h}$ ($A^2A_1$ in $C_{3v}$), is calculated to be 2.41 eV. When the same calculation is performed at the $BCl_3^-$ geometry in Table V, the excitation energy increases to 4.99 eV. Considering that the vertical EA of the $X^2A_2''$ state is $-0.63$ eV by the

present calculation, the vertical EA for the $A^2A_1'$ state is 3.04 eV. Because the vertical EA for the $X^2A_2''$ state is overestimated by about 0.23 eV with Basis-I, the vertical EA of the $A^2A_1'$ state is expected to be reduced to $\sim$2.8 eV. As shown in Fig. 1, the $A^2A_1'$ state is stable relative to the dissociation into BCl and $Cl_2^-$ only. Because this state can be considered to be a temporary resonant state of the anion, the stability should be further tested by some method.[54] Though the stability of this state is not studied here, we think that the $A^2A_1'$ state is likely to be responsible for the experimental fact that the electron attachment rate constant for $BCl_3$ approaches a plateau at an electron collision energy around 2.0 eV.[22]

## IX. CONCLUSIONS

The geometries and spectroscopic properties of the IR-Raman spectra, photoelectron spectrum, and UV-visible spectra are calculated for all possible fragments in the $BCl_3$ plasma that occur below 11 eV, and compared with the experimental results when available. The calculated results with ECP and the associated valence basis set are quite satisfactory for geometrical parameters, vibrational frequencies, ionization potentials, electron affinities, and electronic excitation energies, although the calculated results, especially for anions, might be improved by using more extended basis sets. The present results, however, are adequate to offer a better than semiquantitative analysis of the experimental results. Based upon the calculated results, several possible interpretations are offered about the possible initial steps in the decomposition paths in the $BCl_3$ plasma process.

When the energy of the colliding electron is greater than 11.30 eV, the collision can produce positive ion fragments from $BCl_3$. While the electrons with energy between 10.10 to 11.30 eV can make the $BCl^+$ ion from BCl, electrons with energy from 8.61 to 10.10 eV can produce the $BCl_2^+$ ion from $BCl_2$. For the low-energy electrons, the major results of the collision with $BCl_3$ is likely to be the formation of a metastable excited state of the $BCl_3^-$ ion, and these metastable states will then decompose into fragments. Though $BCl^-$ and the $a^3B_2$ state of $BCl_2^-$ are calculated to be unstable relative to their neutral species, the present study anticipates the existence of important resonant states for these anions.

Low-energy electrons may behave as scavengers of positive ions which are important in chemical reactions used to etch surfaces. On the other hand, $BCl_3$ acts as an alternative scavenger of the low-energy electrons. The low-lying electronic states in $BCl_3^-$ are likely to play an important role in the discharge kinetics of the $BCl_3$ plasma. The detailed role of $BCl^-$ and $BCl_2^-$ offers another challenge for further theoretical and experimental studies.

From the present study, it is now quite clear that decomposition through the electronic state of $BCl_3^-$ is the most probable initial step for a low-energy electron collision. Especially when the energy of the electron is less than 6.3 eV, the electronic states of $BCl_3^-$ offer the only possible initial intermediates for decomposition paths.

Formation of the positive ion, $BCl_3^+$ is another possible initial step when there are electrons with energies larger than 11.7 eV. If the formation of the $BCl_3^+$ ion is promoted by some other ways like Penning ionization, then dissociative electron recombination can be the initial step.

The fluorescence spectrum from the photofragmentation of $BCl_3$ is analyzed based on the calculated results. The first excited state, $A^2B_1$ of $BCl_2$ in the $C_{2v}$ structure, appears to be the origin of the A-band. After all candidates are considered, factoring in possible error bars in calculations and differences between band origins and band maxima, we conclude that the second and the third excited states, $B^2B_2$ and $C^2A_2$, are likely to be responsible for the B- and C-bands, respectively, but this requires some assumption about the fluorescence process that needs futher consideration. However, there are no suitable alternatives. The third excited state in the $D_{\infty h}$ structure, $^2\Sigma_g^+$, is likely to be the source of the D-band.

In this paper we demonstrate that with the aid of modern *ab initio* electronic structure tools, many of the complicated processes and the variety of species that occur in a plasma can yield to a detailed analysis. Coupling electronic structure to dynamics should make it possible to begin to realistically model such plasmas for optimum applications.

## ACKNOWLEDGMENTS

The authors express appreciation to Dr. Alan Garscadden for suggesting the study of $BCl_3$ and for numerous helpful discussions. K. Baeck thanks Dr. Nevin Oliphant and Dr. John D. Watts for their help during this work. Discussions on Sec. VIII with Dr. Marcel Nooijen and Dr. Howard Pritchard are also appreciated. We also thank Dr. Marilyn E. Jacox for a copy of Ref. 26 prior to publication. This work has been supported by the U.S. Air Force Office of Scientific Research, under Grant. No. AFOSR-F49620-93-1-0127. K. Baeck has been partially supported by the Korean Science and Engineering Foundation.

[1] S. J. Pearton, W. S. Hobson, C. R. Abernathy, F. Ren, T. R. Fullowan, A. Katz, and A. P. Perley, Plasma Chem. Plasma Proc. **13**, 311 (1993).
[2] D. Flamm, Solid State Technol. **36**, 49 (1993).
[3] G. J. Sonek and J. M. Ballantyne, J. Vac. Sci. Technol. B **2**, 653 (1984).
[4] R. H. Burton, R. A. Gottscho, and G. Smolinsky, *Dry Etching for Microelectronics*, edited by R. A. Powell (Elsevier, New York, 1984).
[5] G. G. Lister, Vacuum **45**, 525 (1994), and references therein.
[6] D. L. Flamm, V. M. Donnelly, and D. E. Ibbotson, J. Vac. Sci. Technol. B 1, 23 (1983).
[7] K. R. Ryan and I. C. Plumb, Plasma Chem. Plasma Proc. **10**, 207 (1990); W. L. Morgan, *ibid.* **12**, 449,477 (1992).
[8] A. Garscadden, ''Ionization waves in glow discharges,'' in *Gaseous Electronics*, edited by N. Hirsh and H. Oskam (Academic, New York, 1978), Vol. 1, pp. 65–107.
[9] C. A. Moore, G. P. Davis, and R. A. Gottscho, Phys. Rev. Lett. **52**, 538 (1982).
[10] W. L. Morgan, Plasma Chem. Plasma Proc. **12**, 449,477 (1992).
[11] C. K. Birdsall, IEEE Trans Plasma Sci. **19**, 65 (1991).
[12] G. G. Lister, J. Phys. D Appl. Phys. **25**, 1649 (1992).
[13] L. J. Radziemski, Microchem. J. **50**, 218 (1994).
[14] J. Deson, F. Haloua, C. Lalo, A. Rousseau, and V. Veniard, J. Phys. D Appl. Phys. **27**, 2320 (1994).
[15] L. Perelmutter, G. Davara, and Y. Maron, Phys. Rev. E **50**, 3984 (1994).

[16] G. R. Scheller, R. A. Gottscho, T. Intrator, and D. B. Graves, J. Appl. Phys. **64**, 4384 (1988).
[17] F. W. Breitbarth, Plasma Chem. Plasma Proc. **12**, 261 (1992).
[18] G. R. Scheller, R. A. Gottscho, T. Intrator, and D. B. Graves, J. Appl. Phys. **64**, 4384 (1988).
[19] Z. J. Jabbour, K. E. Martus, and K. Becker, Bull. Am. Phys. Soc. **33**, 941 (1988); P. G. Gilbert, R. B. Siegel, and K. Becker, Phys. Rev. A **41**, 5594 (1990).
[20] D. J. Mosteller, Jr., M. L. Andrews, J. D. Clark, and A. Garscadden, J. Appl. Phys. **74**, 2247 (1993); C. B. Zarowin, J. Electrochem. Sci. **130**, 1144 (1983).
[21] J. A. Stockdale, D. R. Nelson, F. J. Davis, and R. N. Compton, J. Chem. Phys. **56**, 3336 (1972); L. G. Christophorou and J. A. Stockdale, J. Chem. Phys. **48**, 1956 (1965).
[22] Z. L. Pertovic, W. C. Wang, M. Suto, J. C. Han, and L. C. Lee, J. Appl. Phys. **67**, 675 (1990).
[23] M. Suto, C. Ye, J. C. Han, and L. C. Lee, J. Chem. Phys. **89**, 6653 (1988).
[24] J. C. Creasey, P. A. Hatherly, I. R. Lambert, and R. P. Tuckett, Mol. Phys. **79**, 413 (1993); H. Biehl, J. C. Creasey, D. M. Smith, R. P. Tuckett, K. R. Yoxall, H. Baumgartel, H. W. Jochims, and U. Rockland, J. Chem. Soc. Faraday Trans. **91**, 3073 (1995); H. Biehl, K. J. Boyle, D. M. Smith, R. P. Tuckett, K. R. Yoxall, K. Codling, P. A. Hatherly, and M. Stankiewicz, *ibid.* **92**, 185 (1996).
[25] J. H. Miller and L. Andrews, J. Am. Chem. Soc. **102**, 4900 (1980); P. Hassanzadeh and L. Andrews, J. Phys. Chem. **97**, 4910 (1993).
[26] M. E. Jacox, K. K. Irikura, and W. E. Thompson, J. Chem. Phys. **104**, 8871 (1996).
[27] D. R. Armstrong and P. G. Perkins, J. Chem. Soc. A 3674 (1971), and references therein.
[28] D. Goutier and L. A. Burnell, Chem. Phys. Lett. **18**, 460 (1973).
[29] J. A. Tossell and J. H. Moore, Int. J. Quant. Chem. **24**, 1117 (1986).
[30] R. J. Bartlett, J. Phys. Chem. **93**, 1697 (1989); R. J. Bartlett and J. F. Stanton, ''Applications of post-Hartree-Fock methods: A tutorial,'' in *Reviews in Computational Chemistry*, edited by D. Boyd and K. Lipkowitz (VCH, New York, 1994), Vol 5, p. 63.
[31] Advanced Concepts in Electronic Structure (ACES II) — A product of the University of Florida Quantum Theory Project, developed by J. F. Stanton, J. Gauss, J. D. Watts, W. J. Lauderdale, and R. J. Bartlett, with contributions from N. Oliphant, P. Szalay, A. Balkova, S. A. Perera, K. Baeck, M. Nooijen, D. Bernholdt, and H. Sekino. The program uses the VMOL integral package written by J. Almlof and P. Taylor and a modified version of the ABACUS integral derivative package of T. U. Helgaker, H. J. Aa. Jensen, J. Olson, P. Jørgensen, and P. Taylor.
[32] H. Sekino and R. J. Bartlett, Int. J. Quantum Chem. Symp. **18**, 255 (1984); J. Geertsen, M. Rittby, and R. J. Bartlett, Chem. Phys. Lett. **164**, 57 (1989); D. C. Comeau and R. J. Bartlett, Chem. Phys. Lett. **207**, 414 (1993); J. F. Stanton and R. J. Bartlett, J. Chem. Phys. **98**, 7029 (1993); *ibid* **98**, 9335 (1993).
[33] J. F. Stanton, M. Rittby, and R. J. Bartlett, J. Chem. Phys. **97**, 5560 (1992). (Fock space MRCC is the same as IP-EOM-CC for principal ionizations.)
[34] M. Nooijen and R. J. Bartlett, J. Chem. Phys. **102**, 3629 (1995).
[35] R. J. Bartlett, J. F. Stanton, and J. D. Watts, in *Advances in Molecular Vibrations and Collision Dynamics*, edited by J. Bowman (JAI Press, London, 1991), Vol. 1, p. 139; J. Gauss and D. Cremer, Adv. Quantum Chem. **23**, 205 (1992).
[36] M. Urban, R. J. Bartlett, and S. A. Alexander, Int. J. Quantum Chem. Quant. Chem. Symp. **26**, 271 (1992).
[37] E. W. Rothe, B. P. Mathur, and G. P. Reck, Inorg. Chem. **19**, 829 (1980).
[38] $(6S6P1D)/[3S3P1D]$ basis sets; M. Dolg, Dissertation, 1989; M. Dolg, U. Wedig, H. Stoll, and H. Preuss, J. Chem. Phys. **86**, 866 (1987).
[39] W. R. Wadt and P. J. Hay, J. Chem. Phys. **82**, 284 (1985).
[40] L. F. Pacios and P. A. Christiansen, J. Chem. Phys. **82**, 2664 (1985).
[41] R. D. Mead, A. E. Stevens, and W. C. Lineberger, *Gas Phase Ion Chemistry*, edited by M. T. Bowers (Academic Press, Orlando, 1984) Vol. 13, p. 213.
[42] P. S. Drzaic, J. Marks, and J. J. Brauman, in Ref. 41, p. 167.
[43] T. H. Dunning, Jr., J. Chem. Phys. **90**, 1007 (1989).
[44] G. D. Purvis, III and R. J. Bartlett, J. Chem. Phys. **76**, 1910 (1982)
[45] R. J. Bartlett, J. D. Watts, S. A. Kucharski, and J. Noga, Chem. Phys. Lett. **165**, 513 (1990).
[46] G. D. Purvis, III, H. Sekino, and R. J. Bartlett, Collect. Czech. Chem. Commun. **53**, 2203 (1988).
[47] M. Rittby and R. J. Bartlett, J. Phys. Chem. **92**, 3033 (1988); J. Gauss, W. J. Lauderdale, J. F. Stanton, J. D. Watts, and R. J. Bartlett, Chem. Phys. Lett. **182**, 207 (1991).
[48] P. C. Hariharan and J. A. Pople, Theor. Chim. Acta **101**, 213 (1973); M. M. Francl, W. J. Hehre, J. S. Binkely, M. S. Gordon, D. J. DeFrees, and J. A. Pople, J. Chem. Phys. **77**, 3654 (1982).
[49] A. Balkova and R. J. Bartlett, J. Chem. Phys. **101**, 8972 (1994).
[50] A. Balkova, L. Meissner, and R. J. Bartlett, J. Chem. Phys. **101**, 8972 (1994).
[51] G. Herzberg, *Spectra of Diatomic Molecules* (Van Nostrand Company, New York, 1950).
[52] JANAF Tables, J. Phys. Chem. Ref. Data, 14, Suppl. 1 (1985).
[53] R. D. Verma, J. Mol. Specrosc. **169**, 295 (1995).
[54] J. S. Chao, M. F. Falcetta, and K. D. Jordan, J. Chem. Phys. **93**, 1125 (1990), and references therein.
[55] V. H. Dibeler and J. A. Walker, Inorg. Chem. **8**, 50 (1969).
[56] L. C. Lee, J. C. Han, and M. Suto, J. Chem. Phys. **91**, 2036 (1989).
[57] K. K. Baeck, J. D. Watts, S. Beck, and R. J. Bartlett, ''Analytical energy gradients with dropped core in CC/MBPT,'' to be published.
[58] H. J. Maria, J. R. McDonald, and S. P. McGlynn, J. Am. Chem. Soc. **95**, 1050 (1973).
[59] A. D. Walsh, J. Chem. Soc., 2301 (1953).
[60] N. Oliphant and R. J. Bartlett, J. Chem. Phys. **100**, 6550 (1994).
[61] H. Basch, Chem. Phys. Lett. **136**, 289 (1987); G. Pacchion, P. Fantucci, and J. Koutecky, *ibid.* **142**, 85 (1987).
[62] Y. M. Hamrick, R. J. Van Zee, and W. Weltner, Jr., J. Chem. Phys. **96**, 1767 (1992); J. S. Tse, *ibid.* **92**, 2488 (1990).
[63] J. F. Stanton, J. Gauss, and R. J. Bartlett, J. Chem. Phys. **94**, 4084 (1991).
[64] J. F. Stanton, J. Gauss, and R. J. Bartlett, J. Chem. Phys. **97**, 5554 (1992).
[65] J. H. Callomon, E. Hirota, K. Kuchitsu, W. J. Lafferty, A. G. Maki, and C. S. Pole, in Landolt–Bornstein, *Numerical Data and Functional Relationships in Science and Technology, New Series, Group II Atomic and Molecular Physics*, edited by K. H. Hellwege and A. M. Hellwege (Springer, New York, 1976), Vol. 7.
[66] K. Iijina and S. Shibata, Bull. Chem. Soc. Jpn. **53**, 1908 (1980).
[67] R. A. Gottscho and C. E. Gaee, IEEE Trans. Plasma Sci. **PS–14**, 92 (1986).
[68] G. Herzberg, *Molecular Spectra and Molecular Structure, II, Infrared and Raman Spectra of Polyatomic Molecules* (Van Nostrand Company, New York, 1960).
[69] D. F. Shriver and B. Swanson, Inorg. Chem. **10**, 1354 (1971).
[70] J. F. Stanton and R. J. Bartlett, J. Chem. Phys. **97**, 5560 (1992).
[71] P. J. Bassett and D. R. Lloyd, J. Chem. Soc. A, 1551 (1971).
[72] A. A. Planckaert, P. Sauvageau, and C. Sandorfy, Chem. Phys. Lett. **20** 170 (1973).
[73] J. D. Watts and R. J. Bartlett, J. Chem. Phys. **101**, 3073 (1994); Chem. Phys. Lett. **233**, 81 (1995); **258**, 581 (1996).
[74] M. Peric and S. D. Peyerimhoff, Mol. Phys. **78**, 855,877 (1993).
[75] R. Nagpal and A. Garscadden, Appl. Phys. Lett. **64**, 1626 (1994).
[76] M. J. Linevsky, E. R. Shull, D. E. Mann, and T. Wartik, J. Am. Chem. Soc. **75**, 3287 (1953); D. E. Mann and L. Fano, J. Chem. Phys. **26**, 1665 (1957).
[77] A. Stork, A. Brandt, and H. Fischer, Ber. **58B**, 643 (1925).